Hindawi
Shock and Vibration
Volume 2019, Article ID 6024916, 13 pages
https://doi.org/10.1155/2019/6024916

Research Article

Analysis of Tangential Nonlinear Vibration on Machine Hydrostatic Slide

Zhongkui Zhang,[1,2] **Feng Gao**,[1] **Yan Li**,[1] **and Han Zhang**[1]

[1]*Key Lab. of NC Machine Tools and Integrated Manufacturing Equipment of the Education Ministry & Key Lab. of Manufacturing Equipment of Shaanxi Province, Xi'an University of Technology, Xi'an 710048, China*
[2]*Facility Horticulture Laboratory of Universities in Shandong, Weifang University of Science and Technology, Shouguang 262700, China*

Correspondence should be addressed to Feng Gao; gf2713@126.com

Received 23 February 2019; Revised 6 August 2019; Accepted 20 August 2019; Published 22 September 2019

Academic Editor: Roger Serra

In this paper, the nonlinear dynamic responses of the hydrostatic slide were investigated and the effects of damping and external force to control the vibration system were discussed. The dynamic model of the system was established, and the tangential vibration equation taking into account nonlinear factors was derived. The heteroclinic orbit parameter equations of the vibration system were solved, and the Melnikov function of vibration system is derived. And the chaos condition and judging criterion of the vibration system were obtained by Melnikov's method. The vibration equation of the hydrostatic slide was solved using the numerical method. The bifurcation diagram, phase diagram, wave diagram of displacement, and Poincaré map were obtained, and the nonlinear dynamic responses were analyzed. Finally validation experiments were conducted, and the results agree well with the results obtained by the Melnikov method and numerical method.

1. Introduction

Hydrostatic slide is widely used in precision machines because of the characteristic of low motion error and high stiffness [1, 2]. Figure 1 shows the structure of the hydrostatic slide. However, the dynamic characteristics of the machine table is changed instantaneously and abruptly during the high-speed start-stop, acceleration to constant-speed conversion, and constant-speed to deceleration conversion because of small friction coefficient and tangential low damping of the hydrostatic slide. In addition, the system is forced to vibrate under the cutting force, ground vibration, residual vibration, and oil film nonlinear fluid fluctuation force which lead to poor stability of the hydrostatic slide in the tangential direction and will affect the positioning accuracy and work effectiveness.

The hydrostatic slide is impacted at the moment of start and stop, so residual vibration is produced. The main reason of the vibration is that the hydrostatic slide has low damping in the moving direction, the quality of moving parts is large, and the rigidity of the transmission parts is small. Based on the Lagrange equation, Chen et al. [3] established the nonlinear dynamic model of the machine feed system and studied the influence of damping on the system. Wang et al. [4] established a nonlinear dynamic model of the machine feed mechanism based on the lumped parameter method, derived the self-excited condition of the system during low-speed motion based on the description function method, proposed the method and control strategy for suppressing self-excitation during low-speed motion, and developed a control scheme to improve the accuracy of low-speed motion. Whalley et al. [5] modeled the X-axis drive system of the milling machine using hybrid, distributed-lumped parameter methods, and the dynamics of the system was also studied. Chen et al. [6] established the dynamic model of the machine feed system with the hybrid element method and

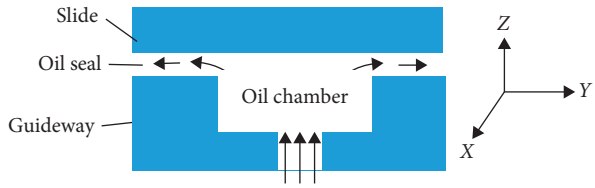

Figure 1: Structure of a hydrostatic slide.

studied the dynamic characteristics of the system. Based on the classical friction model, Bui et al. [7] built the nonlinear friction model of the machine feed system under high-speed motion, and the average contour error of the new friction model was reduced by 26% comparing with the classical friction model. For the vibration caused by external environment, Law et al. [8] studied the suppression of machine vibration by using electrohydraulic actuators. Yang et al. [9] studied the vibration of the heavy-duty machine tool. Er and Tan [10] studied the vibration of machine tools based on experimental modal analysis methods and frequency response functions. Zhang et al. [11] reviewed the vibration characteristics of ultraprecision machine tools during processing and the effect of vibration on surface formation. Otto and Radons [12] studied the vibration and stability of an intermittent turning machine with a circular blade by the frequency domain method. In order to suppress the self-excited vibration, forced vibration, rocking vibration, and vibration caused by machine cutting, viscoelastic dampers can be used to reduce the vibration of the machine tool and typical dampers include magnetorheological dampers and electrorheological dampers [13–20].

However, all of the above models were simplified by replacing the distribution parameters with lumped parameters, replacing the time-varying parameters with quantitative parameters and using the equivalent linear characteristics instead of the nonlinear characteristics. And there are few research reports on the tangential vibration of the hydrostatic slide. In this paper, the influences of damping and external force on the hydrostatic slide tangential vibration were analyzed based on the nonlinear idea.

In this paper, we studied the dynamic behaviors of the machine hydrostatic slide. In the next section, the mathematical model of the machine hydrostatic slide is described and the tangential single-freedom dynamic model equations are derived. In Section 3, the necessary conditions for chaotic motion of the hydrostatic slide are solved by Melnikov's method. Section 4 discusses the dynamic responses of the vibration system with the effects of key system parameters such as damping and external force. Validation experiments are conducted in Section 5. Finally, some conclusions are drawn briefly in Section 6.

2. Theoretical Model

According to the structural properties of the hydrostatic slide system, the system is divided into two parts. The guideway whose rigidity is very high is fixed on the base of the machine. The guideway and the base can be regarded as the whole, which is the first part. The slider is considered to be the second part, which is separated from the guideway by oil film. The quality of the first part is much greater than the other part, so the first part can be considered as the basis when building a dynamic model. This paper focuses on the vibration of the slider in the tangential direction. Figure 2 shows the simplified dynamic model of the hydrostatic slide; K is the stiffness, and C is the damping of the system.

According to the Lagrange equation, the nonlinear vibration equation of the hydrostatic slide in the tangential direction is obtained:

$$M\ddot{X} + C\dot{X} + K\left(X + \varepsilon X^3\right) = p\cos(\omega t), \tag{1}$$

where M is the mass of the hydrostatic slide; $p\cos(\omega t)$ is total exciting force; ω is the frequency of exciting force; ε is the nonlinear coefficient, $0 < \varepsilon \le 1$ [21]; $X, \dot{X}, \ddot{X}$ are the vibration displacement, velocity, and acceleration, respectively.

Equation (1) is rewritten as

$$\ddot{X} + \mu\dot{X} + \alpha X + \beta X^3 - F\cos(\omega t) = 0, \tag{2}$$

where $\mu = (C/M)$, $\alpha = (K/M)$, $\beta = (K\varepsilon/M)$, and $F = (P/M)$.

The dimensionless equation of the system can be written as

$$\ddot{x} + \gamma\dot{x} + X + X^3 = f\cos(\Omega t), \tag{3}$$

where $x = \sqrt{\beta/\alpha}X$, $\gamma = \mu/\sqrt{\alpha}$, $\omega_n = \sqrt{K/M}$, $\tau = \sqrt{\alpha}t$, $\Omega = \omega/\sqrt{\alpha}$, and $f = (F\sqrt{\beta})/(\alpha\sqrt{\alpha})$.

3. Nonlinear Judgment Basis: Melnikov Function Method

Introducing new variables $\dot{X} = Y$, $F = \xi F_1$, and $\mu = \xi\mu_1$, then equation (2) can be transformed into the following form [22–24]:

$$\begin{cases} \dot{X} = Y, \\ \dot{Y} = -\alpha X - \beta X^3 + \xi\left(-\mu_1 Y + F_1\cos(\omega t)\right). \end{cases} \tag{4}$$

Let $\xi = 0$, i.e., $F = 0$ and $\mu = 0$, and the above equation is an undisturbed Hamiltonian system equation, i.e.,

$$\begin{cases} \dot{X} = Y, \\ \dot{Y} = -\alpha X - \beta X^3, \end{cases} \tag{5}$$

setting

$$\begin{cases} \dot{X} = Y = 0, \\ \dot{Y} = -\alpha X - \beta X^3 = 0. \end{cases} \tag{6}$$

Three fixed points were obtained: $(\pm\sqrt{\alpha/\beta}, 0)$ and $(0, 0)$. The characteristic equation of equation (4) is

$$\begin{vmatrix} 0-\lambda & 1 \\ -\alpha - 3\beta X^2 & 0-\lambda \end{vmatrix} = 0, \tag{7}$$

i.e.,

$$\lambda^2 + \alpha + 3\beta X^2 = 0. \tag{8}$$

So $\lambda = \pm\sqrt{3\beta X^2 - \alpha}i$.

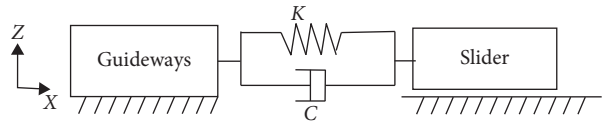

Figure 2: Simplified dynamic model of the hydrostatic slide.

The Hamilton of equation (5) is $H(X,Y) = (1/2)Y^2 + (1/2)\alpha X^2 + (1/4)\beta X^4$.

Heteroclinic orbits can be obtained by solving the following equation:

$$\begin{cases} \dot{X} = Y, \\ H(X,Y) = \dfrac{1}{2}Y^2 + \dfrac{1}{2}\alpha X^2 + \dfrac{1}{4}\beta X^4 = \dfrac{\alpha^2}{4\beta}. \end{cases} \tag{9}$$

So the parametric equations are obtained:

$$\begin{cases} X_i(t) = \pm\sqrt{\dfrac{\alpha}{\beta}}\, th\left(\sqrt{\dfrac{\alpha}{2}}t\right), \\ Y_i(t) = \pm\dfrac{\alpha}{\sqrt{2\beta}}\, \mathrm{sech}^2\left(\sqrt{\dfrac{\alpha}{2}}t\right), \\ i = 1, 2. \end{cases} \tag{10}$$

Melnikov's function is obtained as follows:

$$M_i(t_0) = \int_{-\infty}^{+\infty} f\left(q_i^0(t)\right) \wedge g\left(q_i^0(t)\right)(t + t_0)dt, \tag{11}$$

where g is an additional periodic driving function; f is the nonlinear term function; q^0 is the homoclinic (heteroclinic) trajectory expression; $\wedge$ is the normal projection operator, and the detailed operation is that $a = (a_1, a_2)$ and $b = (b_1, b_2)$:

$$a \wedge b = a_1 b_2 - a_2 b_1. \tag{12}$$

The Melnikov function under perturbation is obtained:

$$\begin{aligned} M_i(t_0) &= \int_{-\infty}^{+\infty} [\delta_1 Y_i(t) + \gamma_1 \cos(t + t_0) Y_i(t)]dt \\ &= \delta_1 \int_{-\infty}^{+\infty} \frac{\alpha^2}{2}\, \mathrm{sech}^4\left(\sqrt{\frac{\alpha}{2}}t\right)dt \\ &\pm \gamma_1 \int_{-\infty}^{+\infty} \frac{\alpha}{\sqrt{2\beta}}\, \mathrm{sech}^2\left(\sqrt{\frac{\alpha}{2}}t\right)\cos(\omega t)dt \\ &\cdot \cos(\omega t_0) = \frac{4\alpha}{3\beta}\sqrt{\frac{\alpha}{2}}\delta_1 \pm \gamma_1 I \cos(\omega t_0), \quad i = 1, 2, \end{aligned} \tag{13}$$

where

$$\begin{aligned} I &= \int_{-\infty}^{+\infty} \frac{\alpha}{\sqrt{2\beta}}\, \mathrm{sech}^2\left(\sqrt{\frac{\alpha}{2}}t\right)\cos(\omega t)dt \cos(\omega t_0) \\ &= \mathrm{Res}\left(\int_{-\infty}^{+\infty} \frac{\alpha}{\sqrt{2\beta}}\, \mathrm{sech}^2\left(\sqrt{\frac{\alpha}{2}}z\right)e^{j\omega z}dt\right). \end{aligned} \tag{14}$$

According to the residue theorem, the analytical expression of I is

$$\begin{aligned} R(z) &= \frac{\varphi(z)}{\psi(z)} = \frac{\alpha}{\sqrt{2\beta}}\, \mathrm{sech}^2\left(\sqrt{\frac{\alpha}{2}}z\right)e^{j\omega z} \\ &= \frac{4\alpha}{\sqrt{2\beta}}\, \frac{e^{(\sqrt{2\alpha}+i\omega)z}}{\left(e^{(\sqrt{2\alpha})z} + 1\right)^2}, \end{aligned} \tag{15}$$

where

$$\begin{cases} \varphi(z) = \dfrac{4\alpha}{\sqrt{2\beta}}e^{(\sqrt{2\alpha}+i\omega)z}, \\ \psi(z) = \left(e^{(\sqrt{2\alpha})z} + 1\right)^2. \end{cases} \tag{16}$$

Select the roads as shown Figure 3. The ordinate value of point p is $\pi/\sqrt{2\alpha}$.

According to the residue theorem,

$$\begin{aligned} \oint R(z)dz &= \int_{l_1} R(z)dz + \int_{l_1} R(z)dz + \int_{l_2} R(z)dz \\ &+ \int_{l_3} R(z)dz + \int_{l_4} R(z)dz \\ &= 2\pi i \sum_{k=1}^{n} \mathrm{Res}[R(z), z_k]. \end{aligned} \tag{17}$$

Based on residue theorem,

$$\mathrm{Res} = \left[\frac{\varphi(z)}{\psi(z)}, z_0\right] = \frac{2\dot{\varphi}(z_0) - 2/3\varphi(z_0)\ddot{\psi}(z_0)}{\left[\ddot{\psi}(z_0)\right]^2}. \tag{18}$$

Calculate $\varphi(z)$ and $\psi(z)$ and their derivatives at point z_0:

$$\begin{cases} \varphi(z_0) = -\dfrac{4\alpha}{\sqrt{2\beta}}e^{(-\pi\omega)/\sqrt{2\alpha}}, \\ \dot{\varphi}(z_0) = -(\sqrt{2\alpha} + i\omega)\dfrac{4\alpha}{\sqrt{2\beta}}e^{(-\pi\omega)/\sqrt{2\alpha}}, \\ \ddot{\psi}(z_0) = 4, \\ \dddot{\psi}(z_0) = 12\sqrt{2}\,\alpha^{3/2}. \end{cases} \tag{19}$$

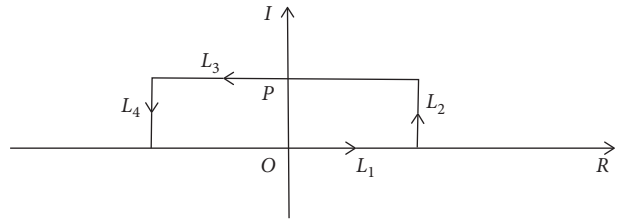

Figure 3: Choice of the roads.

The substitution of (19) into (18) yields

$$\begin{aligned}\text{Res} &= \left[\frac{\varphi(z)}{\psi(z)}, z_0\right] = \frac{2\dot{\varphi}(z_0) - (2/(3\varphi(z_0)\ddot{\psi}(z_0)))}{[\ddot{\psi}(z_0)]^2} \\ &= \frac{\left\{2\left[-(\sqrt{2\alpha} + i\omega)(4\alpha/\sqrt{2\beta})e^{(-\pi\omega)/\sqrt{2\alpha}}\right](4\alpha) - (2/3)\left[-(4\alpha/\sqrt{2\beta})e^{(-\pi\omega)/\sqrt{2\alpha}}\right]12\sqrt{2}\,\alpha^{3/2}\right\}}{(4\alpha)^2} = -\sqrt{\frac{2}{\alpha}}i\omega e^{(-\pi\omega)/\sqrt{2\alpha}}.\end{aligned} \tag{20}$$

Also know

$$\begin{cases} \lim\limits_{R\longrightarrow\infty}\int_{l_1} R(z)dz = I, \\ \lim\limits_{R\longrightarrow\infty}\int_{l_2} R(z)dz = \lim\limits_{R\longrightarrow\infty}\int_{l_4} R(z)dz = 0, \\ \lim\limits_{R\longrightarrow\infty}\int_{l_3} R(z)dz = -\lim\int_{-\infty}^{+\infty}\dfrac{(4\alpha/\sqrt{2\beta})e^{(\sqrt{2\alpha}+i\omega)(x+\sqrt{(2/\alpha)\pi i})}}{\left(e^{(\sqrt{2\alpha})(x+\sqrt{(2/\alpha)\pi i})}+1\right)^2}dx = -e^{\sqrt{(2/\alpha)}\pi\omega}I. \end{cases} \tag{21}$$

The substitution of (20) and (21) into (19) yields

$$I = \sqrt{\frac{2}{\beta}}\pi\omega\,\text{csch}\left(\frac{-\pi\omega}{\sqrt{2\alpha}}\right). \tag{22}$$

The substitution of (22) into (13) yields

$$M_i(t_0) = \frac{4\alpha}{3\beta}\sqrt{\frac{2}{\beta}}\mu_1 \pm F_1\sqrt{\frac{2}{\beta}}\pi\omega\,\text{csch}\left(\frac{\pi\omega}{\sqrt{2\alpha}}\right)\cos(\omega t_0), \quad i = 1, 2. \tag{23}$$

According to the Melnikov theory, setting $M_i(t_0) = 0$, and then the following equation is obtained by using (23):

$$\frac{F_1}{\mu_1} = \frac{2}{3}\frac{\alpha^{2/3}}{\beta^{1/2}}\frac{1}{\pi\omega\,\text{csch}((\pi\omega)/\sqrt{2\alpha})\cos(\omega t_0)}. \tag{24}$$

If $F/\mu > 2/3\,(\alpha^{2/3}/\beta^{1/2})(1/(\pi\omega\,\text{csch}((\pi\omega)/\sqrt{2\alpha})\cos(\omega t_0)))$, the hydrostatic slide may exhibit chaotic motion behavior in the sense of the Smale horseshoe.

The chaotic threshold of the hydrostatic slide system is shown in Figure 4. The hydrostatic slide system may exhibit chaotic dynamic if $C/P < \omega$.

4. Numerical Results and Discussion

Given parameter $M = 35$ kg, $K = 1.0 \times 10^8$ N/m, $\varepsilon = 0.8$, and $\omega = 1$ rad/s. It is known from the calculation results that as long as $P > 1.2728 \times 10^3 C$, the system may exhibit chaotic behavior of the Smale horseshoe sense.

The Matlab/Simulink was used to solve the vibration equation of the hydrostatic slide. Figure 5 shows the Matlab simulated model of the system. The Runge–Kutta algorithm was used to calculate the equation. The relative tolerance is set to 10^{-9}. The influences of damping and external force on hydrostatic slide system tangential vibration properties were analyzed by the numerical simulation method.

4.1. Influence of External Force on System Nonlinearity. Let $C = 0.2$ N·s/m and $\omega A = 1$ rad/s, and external force increased from 0 N to 1000 N. Figures 6–9 shows the bifurcation diagram, phase diagram, Poincaré map, and the wave diagram of displacement, respectively, on the hydrostatic slide.

When $P = 20$ N and $P = 100$ N, the bifurcation diagrams and Poincaré diagrams revealed that the vibration

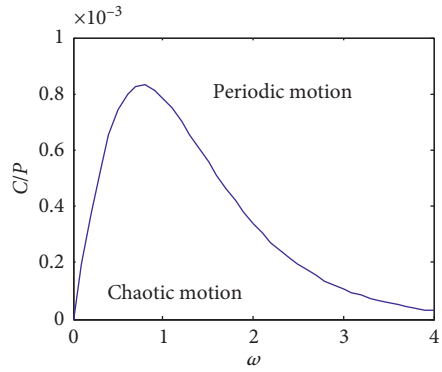

Figure 4: Chaos critical curve of the hydrostatic slide.

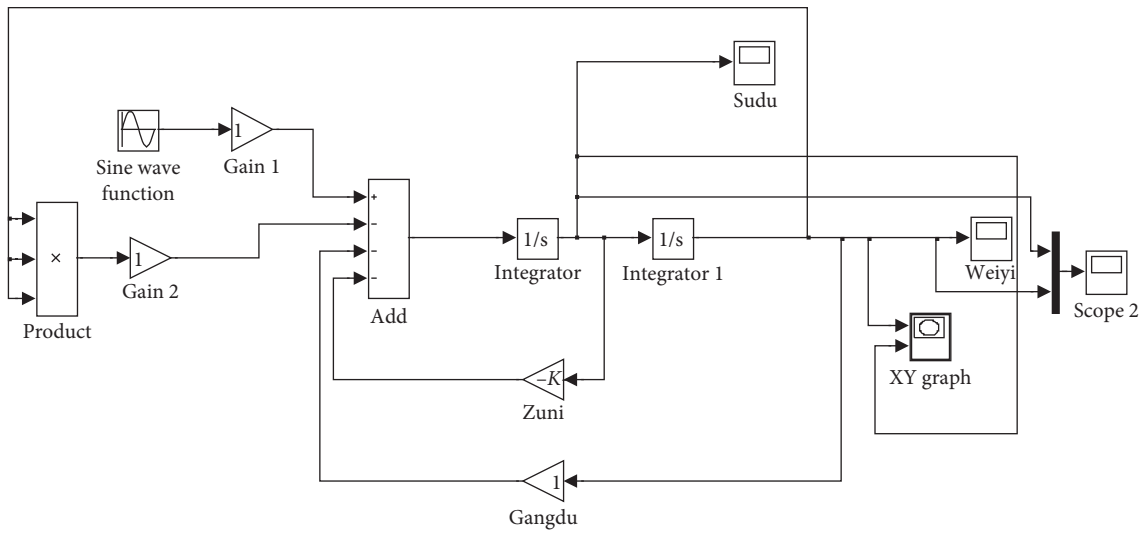

Figure 5: Simulated model of the system.

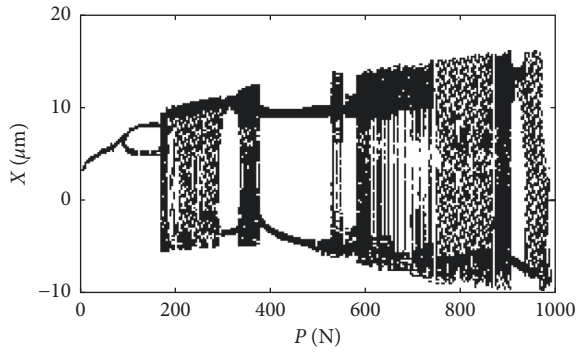

Figure 6: Bifurcation diagram with P as parameter.

characteristics of the hydrostatic slide was period n; When $P = 260$ N, the vibration characteristics of the system was chaotic; when $P = 450$ N, the vibration characteristics of the system was period n again; when $P = 600$ N and $P = 900$ N, the system completely enters chaotic motion. Obviously the Matlab/Simulink results were consistent with the result judged by the Melnikov method. It is known from the displacement waveform diagram that the oscillation period also changes as the external force changing. As the external force increases from 0 to 1000 N, the vibration characteristic of hydrostatic slide goes from the period n to the chaos to the period n and finally to chaos completely. During the chaotic process, there are windows with period n, and that was typical chaotic motion characteristics.

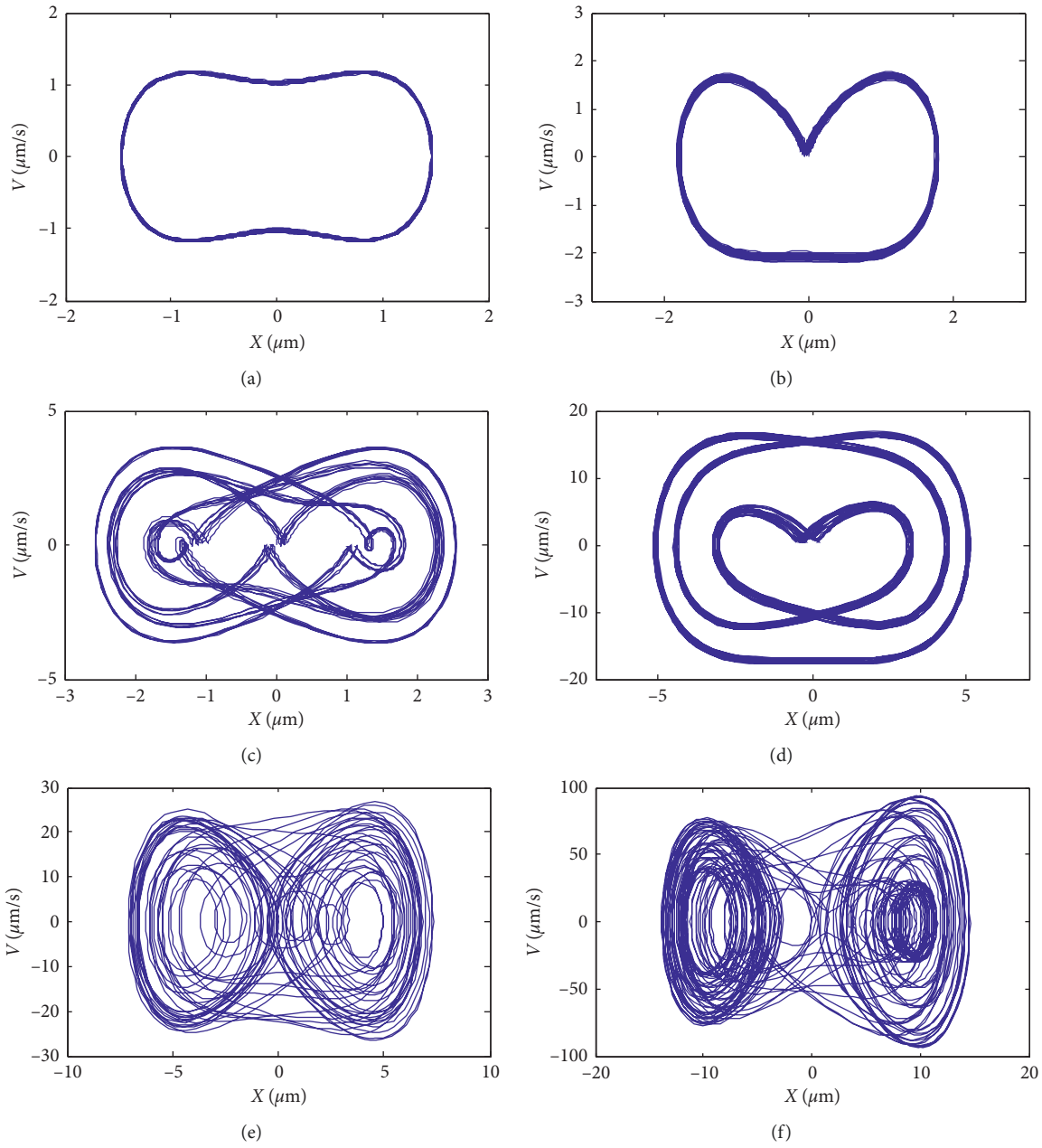

Figure 7: Phase diagram. (a) $P = 20$, (b) $P = 100$, (c) $P = 260$, (d) $P = 450$, (e) $P = 600$, and (f) $P = 900$.

4.2. Influence of Damping on System Nonlinearity. Let $P = 9000$ N and $\omega = 1$ rad/s, and damping increased from 0 to 300 N·s/m. Figures 10–13 shows the bifurcation diagram, phase diagram, Poincaré map, and the wave diagram of displacement, respectively.

When $C = 5$ N·s/m and $C = 7$ N·s/m, the bifurcation diagrams and Poincaré diagrams reveal that the vibration characteristics of the hydrostatic slide was chaotic, and it is consistent with the Melnikov chaos criterion. When $C = 100$ N·s/m, the hydrostatic slide vibration characteristics were chaotic and accompanied by period n windows. When $C = 150$ N·s/m, the chaotic characteristics begin to weaken and exhibited stronger periodicity. When $C = 220$ N·s/m and $C = 280$ N·s/m, the vibration characteristic of the hydrostatic slide was doubling n, and the vibration was stable. It was derived from the displacement waveform diagram that, as the damping increases, the amplitude of the vibration decreases.

4.3. Discussion on Vibration of Machine Hydrostatic Slide. It was concluded from the above analyses that the damping and external force can affect the dynamic responses of the hydrostatic slide. The system motion goes through a process (period $n \longrightarrow$ chaos $\longrightarrow$ period $n \longrightarrow$ chaos) with the external force increasing from 0 to 1000 N, and the amplitude

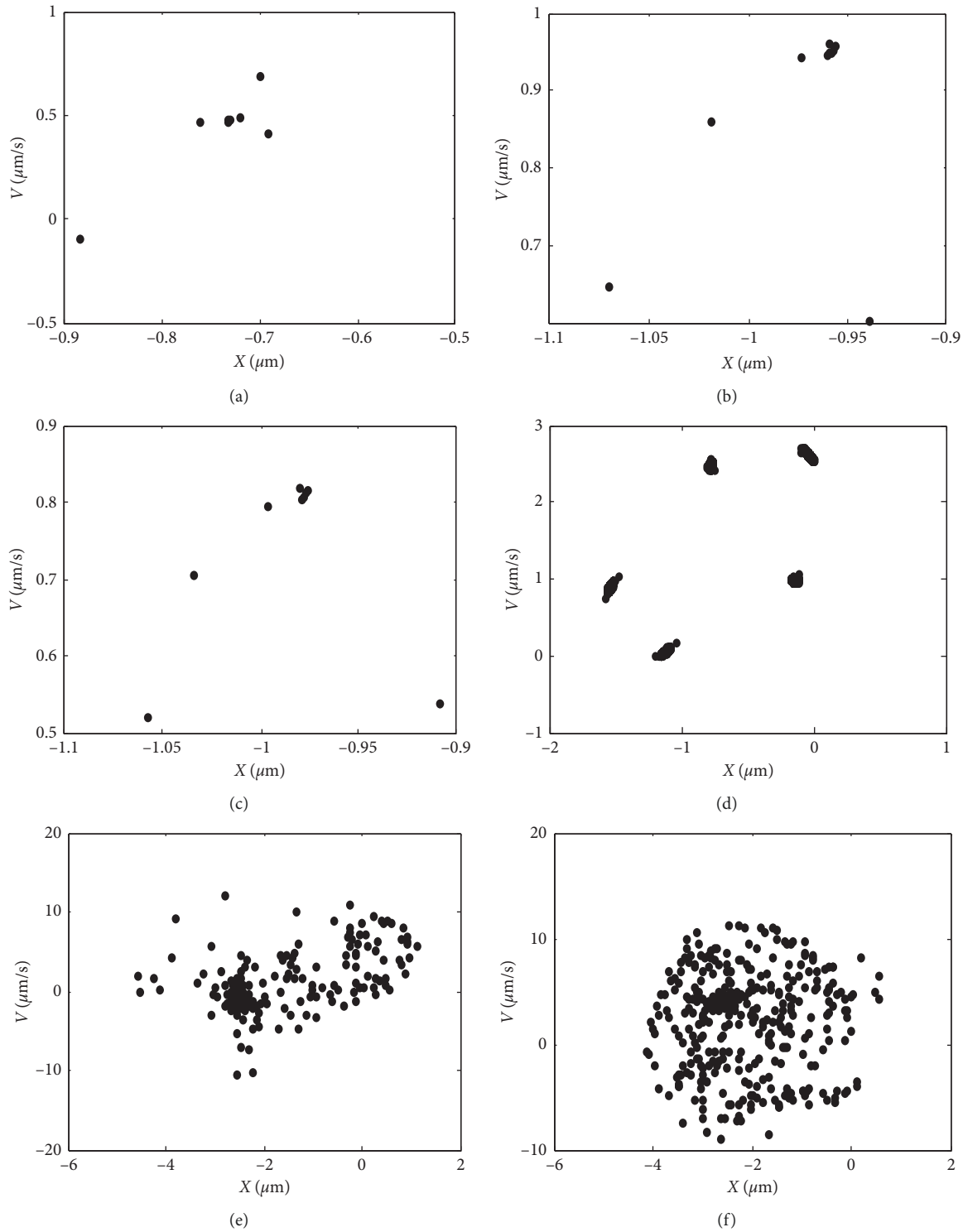

Figure 8: Poincaré map. (a) $P = 20$, (b) $P = 100$, (c) $P = 260$, (d) $P = 450$, (e) $P = 600$, and (f) $P = 900$.

increases. With the increasing damping, the system takes the general form (chaos $\longrightarrow$ period n) and the amplitude decreases. In fact, the greater the external force and the smaller the damping, the more likely the chaotic motion will occur in the vibration system and that is consistent with the result judged by the Melnikov method. Therefore, in order to reduce the vibration of the machine hydrostatic slide, it is necessary to increase the damp by external dampers [13, 15, 25]. And the vibration characteristics of the hydrostatic slide can be altered by adjusting parameters to make the system enter chaotic vibration or avoid chaotic vibration.

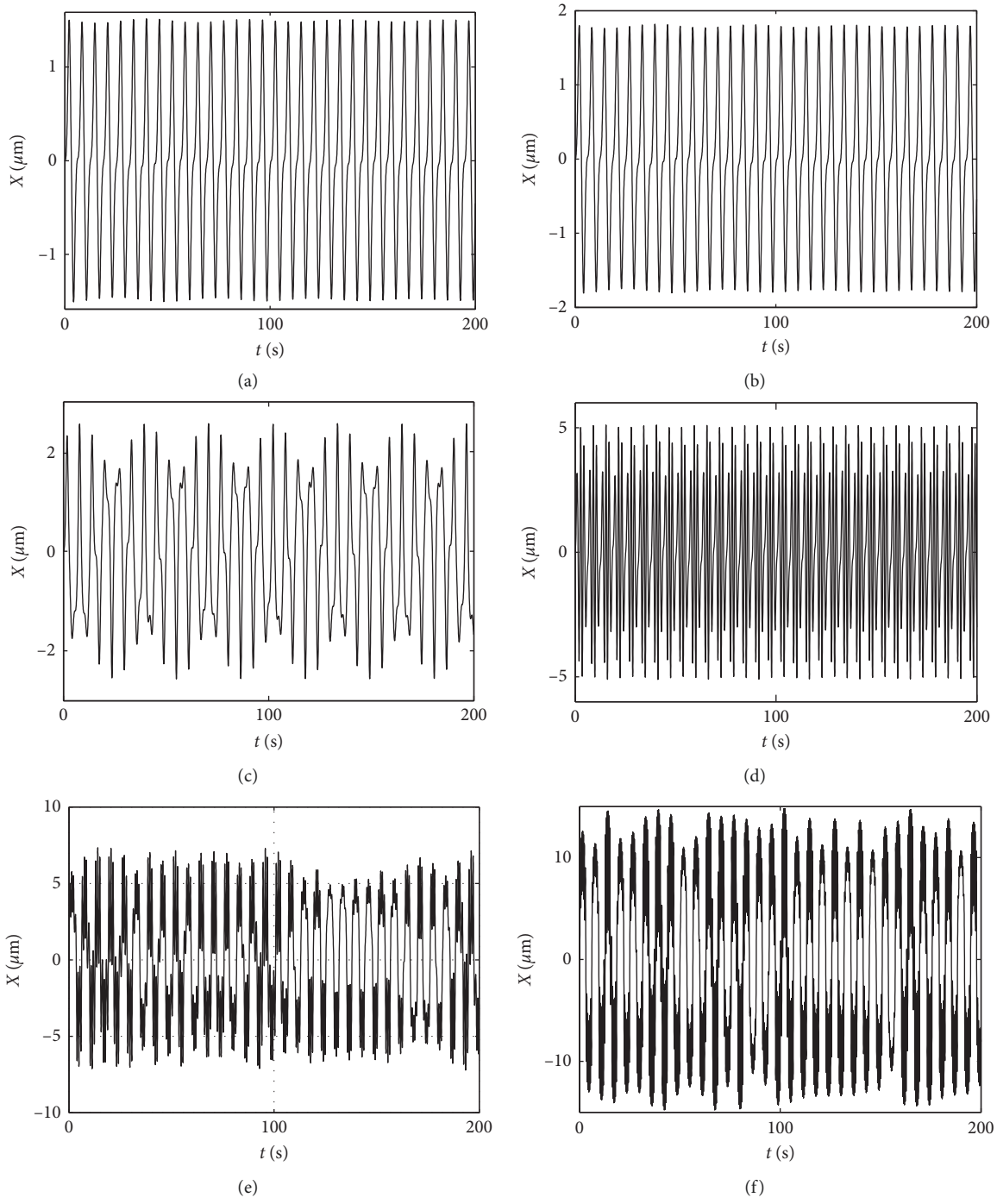

Figure 9: Wave diagram of displacement. (a) $P = 20$, (b) $P = 100$, (c) $P = 260$, (d) $P = 450$, (e) $P = 600$, and (f) $P = 900$.

5. Experimental Verification

The previous analytical results were verified on the hydrostatic slide test platform. The slide was excited by using a hammer, and the test adopted a single-point pick-up multipoint excitation method. The tangential vibration displacement was measured by the Dytran accelerometer. Figure 14 shows the time-domain waveform under case 2, and Figure 15 shows the FFT (fast Fourier transformation) spectrum under cases 1, 2, 3, and 4. The case represents the position of the hydrostatic slide, and cases 1, 2, 3, and 4 represent distance from the slide to the end of the guide is 0 mm, 100 mm, 200 mm, and 300 mm, respectively. It can be concluded from the tangential time-domain waveform that the slide tangential vibration was aperiodic. There is a plurality of approximately overlapping peak positions on the acceleration FFT spectrogram as the natural frequencies. The amplitude is not discrete nor is it a constant

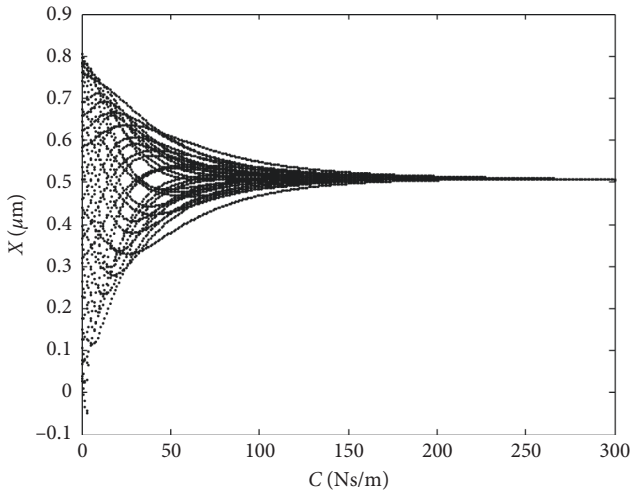

Figure 10: Bifurcation diagram with C as parameter.

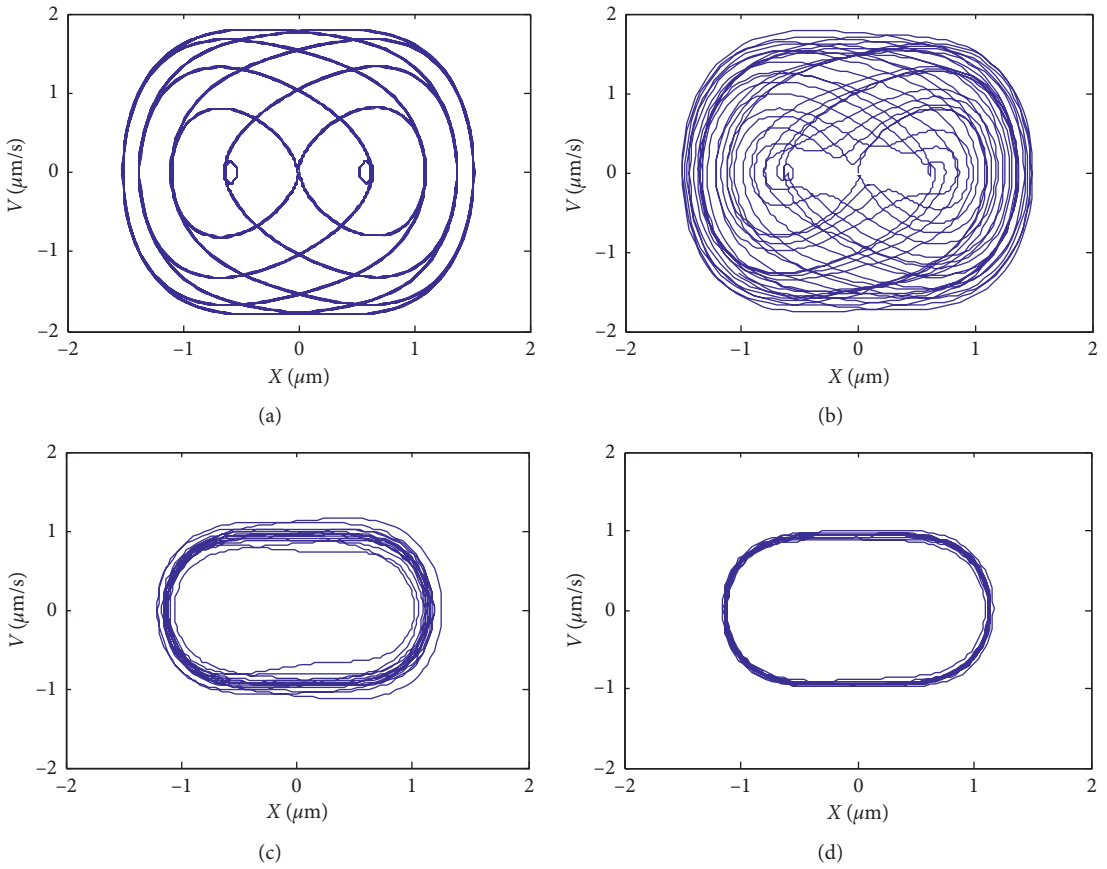

Figure 11: Continued.

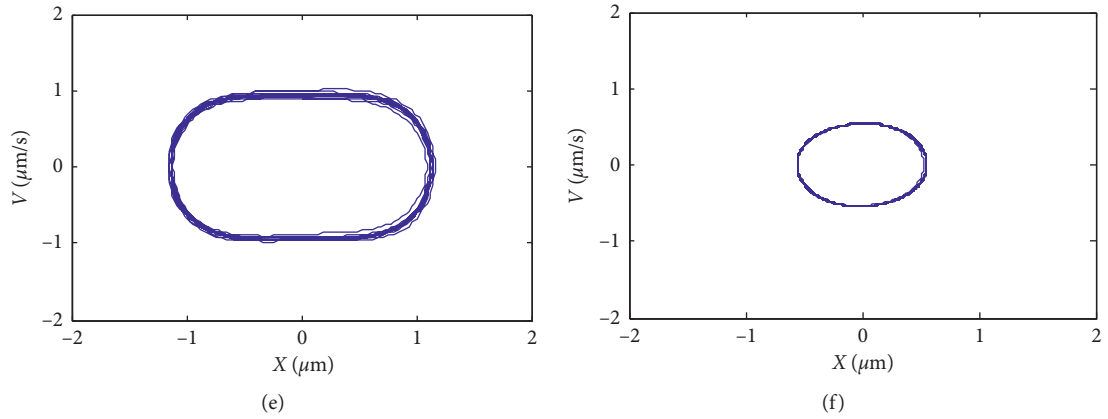

Figure 11: Phase diagram. (a) $C = 5$, (b) $C = 7$, (c) $C = 150$, (d) $C = 200$, (e) $C = 220$, and (f) $C = 280$.

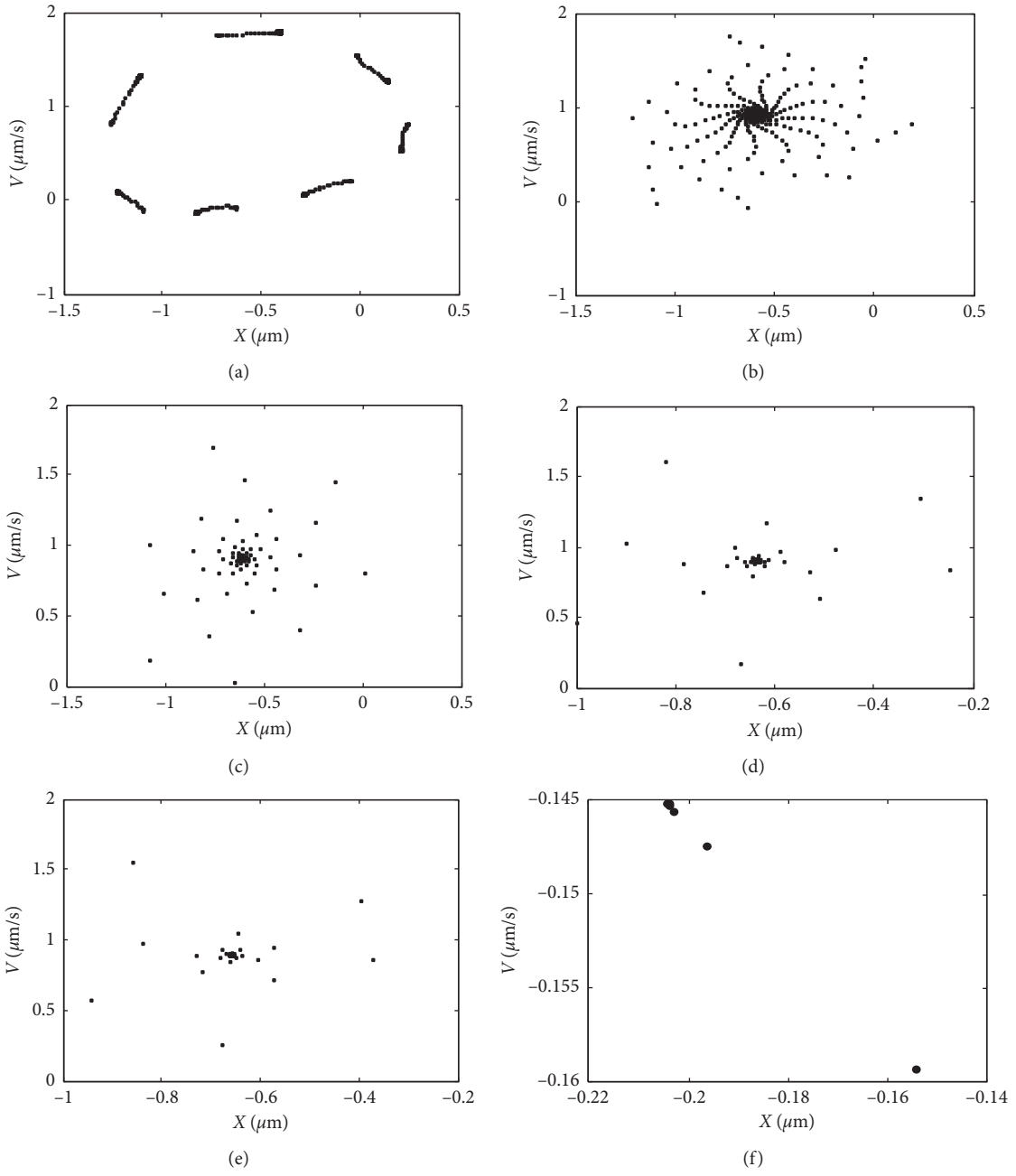

Figure 12: Poincaré map. (a) $C = 5$, (b) $C = 7$, (c) $C = 150$, (d) $C = 200$, (e) $C = 220$, and (f) $C = 280$.

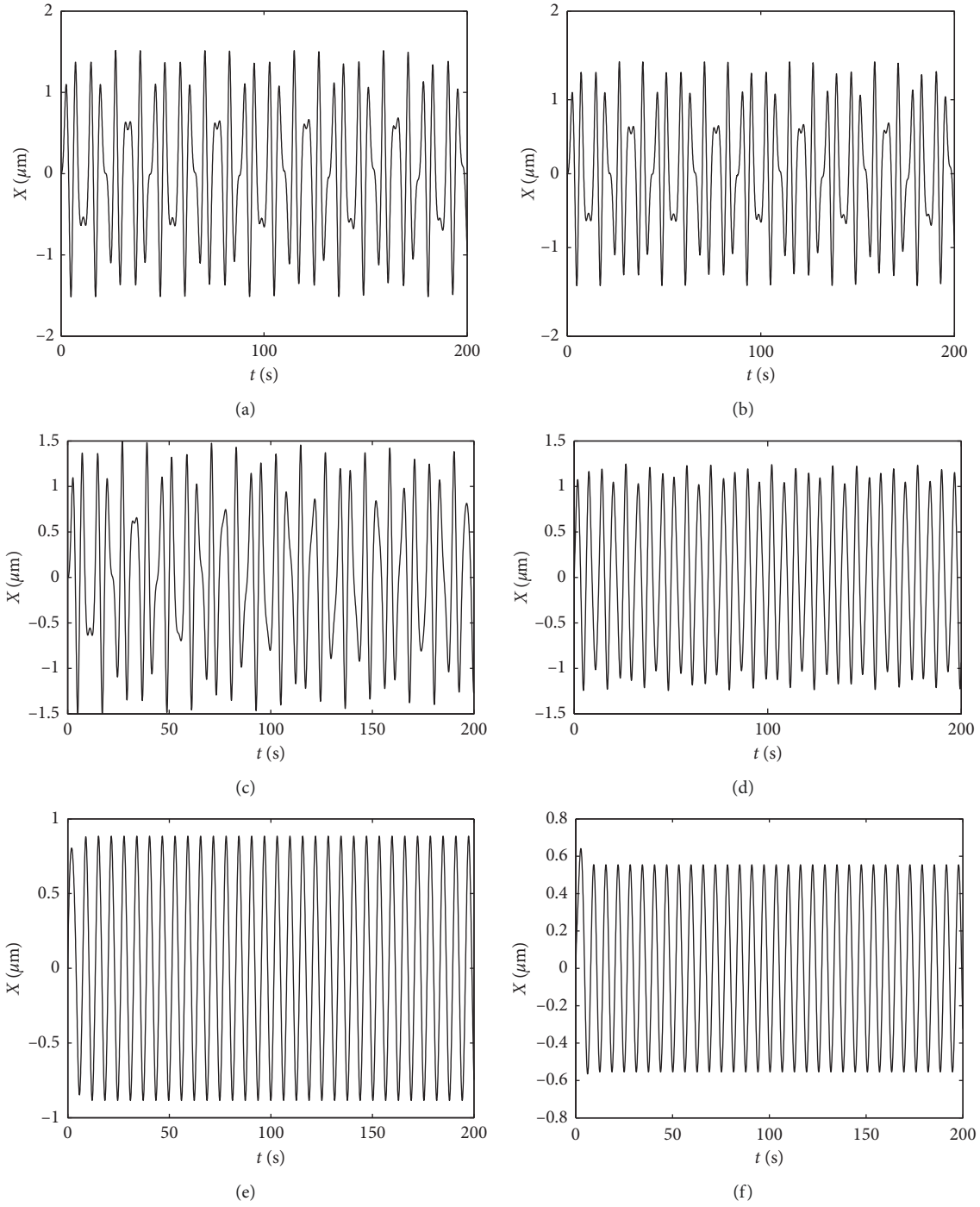

Figure 13: Wave diagram of displacement. (a) $C = 5$, (b) $C = 7$, (c) $C = 150$, (d) $C = 200$, (e) $C = 220$, and (f) $C = 280$.

spectrum, but a continuum with spikes. Judging from these characteristics, the vibration of the hydrostatic slide was neither linear nor random, but nonlinear, which is consistent with the spectral characteristics of the chaotic motion. So the experimental results agree with the results obtained by the Melnikov method and numerical simulation.

6. Conclusions

The nonlinear dynamic responses of the vibration system with the effects of key parameters such as damping and external force were investigated using a single-freedom dynamic model. The chaos condition and judging criterion of the vibration system were obtained by Melnikov's method.

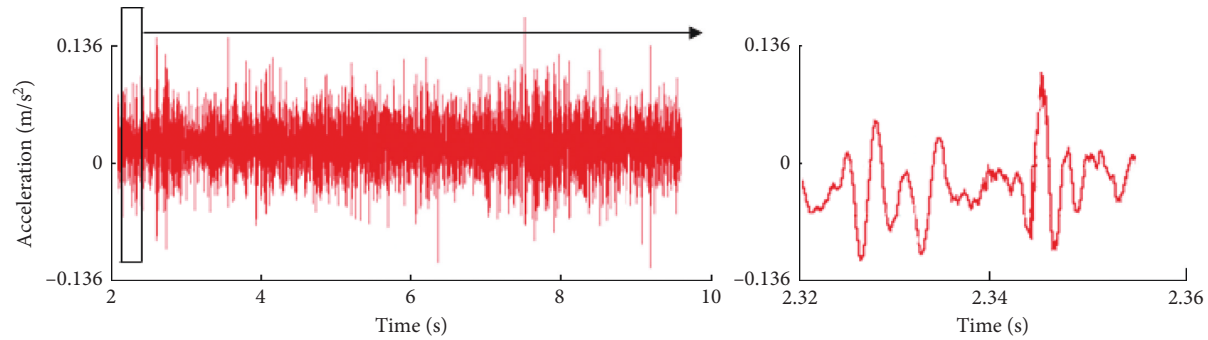

Figure 14: Tangential acceleration time-domain diagram.

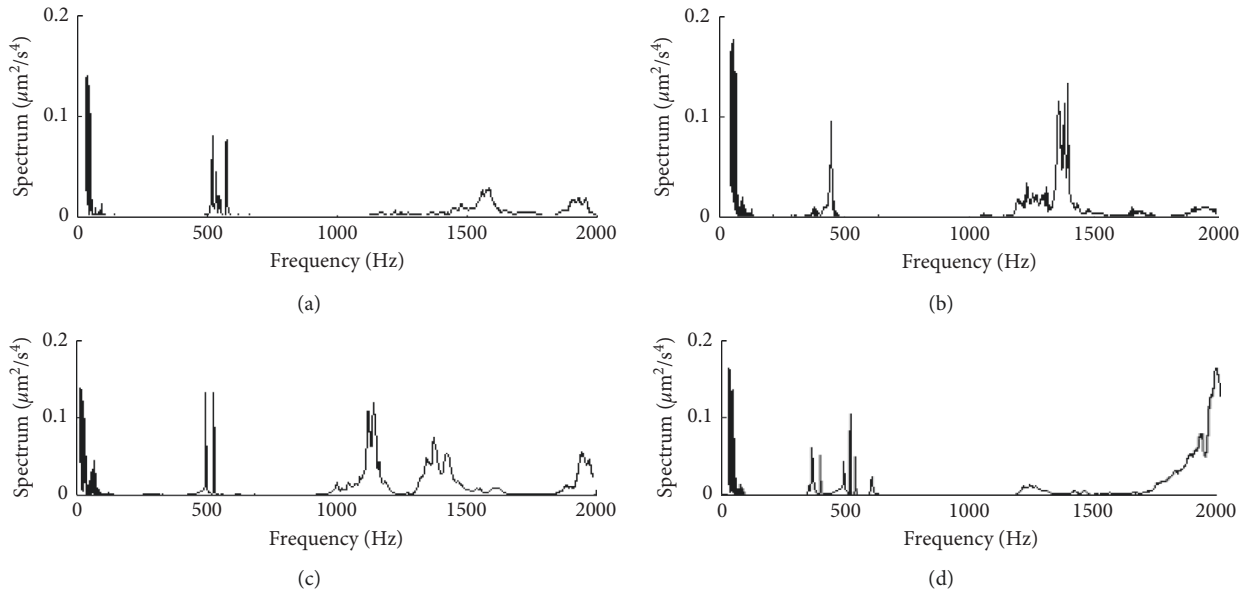

Figure 15: Tangential FFT spectrogram. (a) Case 1, (b) case 2, (c) case 3, and (d) case 4.

(1) The Melnikov method was an effective analytical method to calculate the chaos threshold of dynamic systems, and the chaotic critical condition of the hydrostatic slide system was given by the method

(2) Theoretical and experimental results showed that the vibration of hydrostatic slide system was nonlinear and the system exhibited various types of motion including periodic n and chaotic motions

(3) The chaotic motion of the Matlab/Simulink experiment was of more digital characteristics

Overall, the researches in this paper can not only understand the dynamic response of the machine hydrostatic slide system but also provide some reference to suppress vibration, design, and optimize the vibration system.

Data Availability

The data used to support the findings of this study are included within the article.

Conflicts of Interest

The authors declare that there are no conflicts of interest regarding the publication of this paper.

Acknowledgments

This work was financially supported by the National Natural Science Foundation of China (NSFC) (No. 51775432) and the Science and Technology Project of Weifang University of Science and Technology, China (No. 2018KJWZ08).

References

[1] J. Hwang, C.-H. Park, W. Gao, and S.-W. Kim, "A three-probe system for measuring the parallelism and straightness of a pair of rails for ultra-precision guideways," *International Journal of Machine Tools and Manufacture*, vol. 47, no. 7-8, pp. 1053–1058, 2007.

[2] Z. Wang, W. Zhao, Y. Chen, and B. Lu, "Prediction of the effect of speed on motion errors in hydrostatic guideways," *International Journal of Machine Tools and Manufacture*, vol. 64, pp. 78–84, 2013.

[3] J. L. Chen, N. C. Liu, W. T. Geng, H. R. Zeng, and J. R. Yang, "Analysis of the influence on nonlinear vibration about structural parameters of ball screw on feed system," *Machine Design and Research*, vol. 33, pp. 87–90, 2017, in Chinese.

[4] J. P. Wang, A. Wang, and Z. L. Jing, "Low speed motion stability analysis of mechanical system based on internal feedback," *Mechanical Science and Technology*, vol. 20, pp. 819–832, 2001, in Chinese.

[5] R. Whalley, M. Ebrahimi, and A. A. Abdul-Ameer, "Hybrid modelling of machine tool axis drives," *International Journal of Machine Tools and Manufacture*, vol. 45, no. 14, pp. 1560–1576, 2005.

[6] J. S. Chen, Y. K. Huang, and C. C. Cheng, "Mechanical model and contouring analysis of high–speed ball-screw drive system with compliance effect," *International Journal of Advanced Manufacturing Technology*, vol. 24, pp. 241–250, 2004.

[7] B. D. Bui, N. Uchiyama, and K. R. Simba, "Contouring control for three-axis machine tools based on nonlinear friction compensation for lead screws," *International Journal of Machine Tools and Manufacture*, vol. 108, pp. 95–105, 2016.

[8] M. Law, M. Wabner, A. Colditz, M. Kolouch, S. Noack, and S. Ihlenfeldt, "Active vibration isolation of machine tools using an electro-hydraulic actuator," *CIRP Journal of Manufacturing Science and Technology*, vol. 10, pp. 36–48, 2015.

[9] M. Yang, L. Gui, Y. Hu, G. Ding, and C. Song, "Dynamic analysis and vibration testing of CFRP drive-line system used in heavy-duty machine tool," *Results in Physics*, vol. 8, pp. 1110–1118, 2018.

[10] P. V. Er and K. K. Tan, "Machine vibration analysis based on experimental modal analysis with radial basis functions," *Measurement*, vol. 128, pp. 45–54, 2018.

[11] S. J. Zhang, S. To, G. Q. Zhang, and Z. W. Zhu, "A review of machine-tool vibration and its influence upon surface generation in ultra-precision machining," *International Journal of Machine Tools and Manufacture*, vol. 91, pp. 34–42, 2015.

[12] A. Otto and G. Radons, "Stability analysis of machine tool vibrations in the frequency domain," *IFAC-Papers Online*, vol. 48, no. 12, pp. 328–333, 2015.

[13] T. Aoyama and I. Inasaki, "Application of electrorheological fluid dampers to machine tool elements," *CIRP Annals*, vol. 46, no. 1, pp. 309–312, 1997.

[14] G. Bianchi, S. Cagna, N. Cau, and F. Paolucci, "Analysis of vibration damping in machine tools," *Procedia CIRP*, vol. 21, pp. 367–372, 2014.

[15] J. Fei, B. Lin, S. Yan et al., "Chatter mitigation using moving damper," *Journal of Sound and Vibration*, vol. 410, pp. 49–63, 2017.

[16] S. Ghorbani, V. V. Kopilov, N. I. Polushin, and V. A. Rogov, "Experimental and analytical research on relationship between tool life and vibration in cutting process," *Archives of Civil and Mechanical Engineering*, vol. 18, no. 3, pp. 844–862, 2018.

[17] A. H. H. Hosseinabadi and Y. Altintas, "Modeling and active damping of structural vibrations in machine tools," *CIRP Journal of Manufacturing Science and Technology*, vol. 7, no. 3, pp. 246–257, 2014.

[18] R. Kishore, S. K. Choudhury, and K. Orra, "On-line control of machine tool vibration in turning operation using electro-magneto rheological damper," *Journal of Manufacturing Processes*, vol. 31, pp. 187–198, 2018.

[19] K. Mori, D. Kono, I. Yamaji, and A. Matsubara, "Vibration reduction of machine tool using viscoelastic damper support," *Procedia CIRP*, vol. 46, pp. 448–451, 2016.

[20] K. Mori, D. Kono, I. Yamaji, and A. Matsubara, "Modelling of viscoelastic damper support for reduction in low frequency residual vibration in machine tools," *Precision Engineering*, vol. 50, pp. 313–319, 2017.

[21] Y. Z. Liu and L. Q. Chen, *Nonlinear Vibration*, Higher Education Press, Beijing, China, 2001, in Chinese.

[22] J. B. Li and F. J. Chen, *Chaos, Melnikov Method and New Development*, Science Press, Beijing, China, 2012, in Chinese.

[23] W. G. Zhu, *Nonlinear Thermo-Electro-Magnetic Vibration and Chaos of Rectangular Thin Plate*, Yanshan University, Qinhuangdao, China, 2011, in Chinese.

[24] J. Q. Zhou and Y. Y. Zhu, *Nonlinear Oscillation*, Xi'an Jiaotong University Press, Xi'an, China, 2001, in Chinese.

[25] Z. Zhang, F. Gao, Y. Li, and H. Zhang, "Dynamic and stability analysis of the machine hydrostatic slide with magneto-rheological damper," *Shock and Vibration*, vol. 2019, Article ID 3605830, 11 pages, 2019.